Biosensors and Bioelectronics 41 (2013) 302–308

Contents lists available at SciVerse ScienceDirect

Biosensors and Bioelectronics

journal homepage: www.elsevier.com/locate/bios

Electrophoretic build-up of multi nanoparticle array for a highly sensitive immunoassay

Jin-Hee Han [a], Hee-Joo Kim [b], L. Sudheendra [a], Elizabeth A. Hass [a], Shirley J. Gee [b], Bruce D. Hammock [b], Ian M. Kennedy [a,*]

[a] Department of Mechanical and Aerospace Engineering, University of California, Davis, California, CA 95616, USA
[b] Department of Entomology, University of California, Davis, California, CA 95616, USA

ARTICLE INFO

Article history:
Received 4 June 2012
Received in revised form
7 August 2012
Accepted 17 August 2012
Available online 6 September 2012

Keywords:
Nanoarray
Immunoassay
Electrophoretic particle entrapment system
3-phenoxybenzoic acid (3-PBA)

ABSTRACT

One of the challenges in shrinking immunoassays to smaller sizes is to immobilize the biological molecules to nanometer-scaled spots. To overcome this complication, we have employed a particle-based immunoassay to create a nanostructured platform with a regular array of sensing elements. The technique makes use of an electrophoretic particle entrapment system (EPES) to immobilize nanoparticles that are coated with biological reagents into wells using a very small trapping potential. To provide useful information for controlling the trapping force and optimal design of the nanoarray, electrophoretic trapping of a nanoparticle was modeled numerically. The trapping efficiency, defined as the fraction of wells occupied by a single particle, was 91%. The performance of the array was demonstrated with a competitive immunoassay for a small molecule analyte, 3-phenoxybenzoic acid (214.2 g mole^{-1}). The limit of detection determined with a basic fluorescence microscope was 0.006 μg l^{-1} (30 pM); this represented a sixteen-fold improvement in sensitivity compared to a standard 96-well plate-based ELISA; the improvement was attributed to the small size of the sample volume and the presence of light diffraction among factors unique to this structure. The EPES/nanoarray system promises to offer a new standard in applications that require portable, point-of-care and real-time monitoring with high sensitivity.

1. Introduction

Microarrays have facilitated many breakthroughs in the life sciences by identifying specific gene sequences or protein analytes. The multiplexed technology used in microarrays allows for simultaneous detection of different analytes on a single chip with lower detection limits than conventional laboratory assays (i.e. polymerase chain reaction or enzyme-linked immunosorbent assay) (Chan et al., 2004). Chip-type sensing has also shown potential for use as a point-of-care or real-time assay. These successes have opened the door for research into clinical diagnosis or therapeutic treatment of numerous diseases. To build on these successes, recent research has been moving to the much smaller, or "nano" world. In the cases of screening of diseases or cancer biomarkers using proteomic based approaches, the sample sizes can be extremely limited. This requires that the level of detection be as low as possible. However, nanoarray technology still has some technical difficulties to overcome. Among the most difficult challenges is the need to immobilize small biomolecules on specific nano-sized spots for detecting targets. It is almost impossible to use conventional methods for immobilizing antibodies or proteins onto nanoarrays by using surface modification techniques (e.g. self assembly monolayers) (Schwartz, 2001), although there has been some success building nanoarrays that consist of self-assembled DNA blocks (Liu et al., 2005).

Currently, dip-pen nanolithography has been the most useful method that can directly immobilize biological molecules to nanospots with 100 nm minimum resolutions (Lee et al., 2004; Ginger et al., 2004). However, it requires considerable amounts of time because the solution moves from a tip to the surface mostly by diffusion (Salaita et al., 2005). The method also needs to carefully control environmental conditions such as humidity (Sanedrin et al., 2010). A small number of studies have demonstrated immobilization of biological molecules in an array using particles for immunoassays. Particle-based immunoassays have steadily gained popularity as a solid-phase for antibody immobilization owing to the ease of immobilization of antibodies—the surface area, surface charge, chemical groups and choice of signal transduction can be readily controlled, allowing increased possibilities for antibody immobilization, characterization and detection (Wilson et al., 2006; Haukanes and Kvam, 1993). Many of these features are essential ingredients in increasing sensitivity and lowering the limit of detection (Kusnezow et al., 2006).

Chang et al. (2009) demonstrated electrophoretic trapping of a single microparticle coated with alkaline phosphatase for electrochemical measurement. However, their techniques required complicated

* Corresponding author. Tel.: +1 530 752 2796; fax: +1 530 752 4158.
E-mail address: imkennedy@ucdavis.edu (I.M. Kennedy).

0956-5663/$ - see front matter © 2012 Elsevier B.V. All rights reserved.
http://dx.doi.org/10.1016/j.bios.2012.08.042

and time-consuming fabrication procedures for loading electrodes into micro-scale-patterns. Juan et al. (2009) demonstrated non-invasive optical trapping of a single 53 nm-nanoparticle into a nanowell using a reduced laser intensity. Their method may be useful in avoiding damage to biological reagents coated on particles due to low optical intensity. However, optical trapping is still complicated and expensive. In addition, it may not be suitable for array-type biosensors, which can include dozens or hundreds, or even many thousands, of trapping spots. Powell and Yoon (2006) demonstrated the method of trapping nanoparticles coated with biological samples into nanowells patterned on a p-doped silicon wafer using electrostatic interactions between the surface charge of the particle and the silicon wafer. This method may lead to easier fabrication and trapping—unfortunately it is impossible to control the trapping force in order to manipulate variously charged particles due to the fixed surface charge at the silicon wafer. Furthermore, considerable numbers of particles may be lost during hydrodynamic rinsing.

In this study, our primary objective was to develop a new method that effectively trapped nanoparticles conjugated with biological reagents into specific locations using electrophoresis. To obtain useful information about optimal trapping forces and the design of the nanoarray, the electrophoresis of nanoparticles into nanowells was simulated by a numerical method. The second objective was to demonstrate the performance of the nanoarray as an immuno-platform by quantifying the metabolic product of some pyrethroid insecticides using a competitive immunoassay. Several compounds in the pyrethroid class of insecticides have transitioned from expensive insecticides to commodity chemicals that are the most widely used insecticides worldwide, thus raising the need for environmental markers of their use (Shan et al., 2004; Laffin et al., 2010). Pyrethroids are also widely used in bed nets to control insect vectors of diseases such as malaria (Zaim et al., 2000; Sharma et al., 2009). These uses also raise the possibility of human exposure. Fortunately, 3-phenoxybenzoic acid (3-PBA) is a marker of both environmental presence and human exposure to the major pyrethroids used in the world (Ueyama et al., 2009). Therefore, developing a highly effective analytical technique to detect this analyte is important for environmental monitoring and human health risk assessment.

2. Experimental

2.1. Chip fabrication

Indium tin oxide (ITO) coated glass wafer (catalog no. CG-81N-1515; Resistance: 30–60 Ω; Delta Technologies, Stillwater, MN, USA) was selected for its electrical and optical properties; ITO is a solid material that exhibits excellent electrical conductivity and optical transparency. Before coating the resist, the wafer was washed with acetone (Sigma-Aldrich, St. Louis, MO, USA) and fully spin-dried. LOL-2000 (Microchem, Newton, MA, USA) was spin-coated on the wafer at 6500 rpm for 45 s followed by being baked at 180 °C for 300 s. After cooling the wafer, 2% 950 PMMA A2 (Microchem) was spin-coated on the LOL–ITO–glass wafer at 500 rpm for 5 s followed by 3000 rpm for 45 s. The wafer was then baked on a hot plate at 180 °C for 80 s. Eventually the bi-layer coating procedure made a total 240 nm thickness coating (85 nm PMMA and 155 nm LOL-2000). The thickness was measured by an ellipsometer (Auto EL-2, Rudolph Research Analytical, Hackettstown, NJ, USA). The coated wafer was cut into 37.5 mm × 25 mm chips. The chip was patterned using a scanning electron microscope (SEM) equipped with a nanometer pattern generation system (NPGS, FEI 430 NanoSEM electron beam lithography system, FEI, Hillsboro, OR, USA) at 30 KeV, 33 pA beam current and 1.2 spot size. The chip was then developed using 1:3 methyl isobutyl ketone (MIBK, Sigma)/isopropyl alcohol (IPA, Mallinckrodt Baker, Phillipsburg, NJ, USA) for 90 s followed by being rinsed with IPA for 60 s. To fully eliminate LOL-2000 residue that remained on the ITO surface, additional developing was performed by sonicating the chip in 1:5:5 CD-26 (tetramethylammonium hydroxide, Microchem):H_2O:IPA for 15 s. The chip was then rinsed with deionized (DI) water and dried. Finally, 12 × 12 arrays with 230 nm-wells and 4 μm spacing were patterned on a 50 μm × 50 μm square

2.2. Immunoreagents and buffers

The detailed synthesis of the antibody specific to 3-PBA and competing hapten were previously described by Shan et al. (2004). Briefly, 3-PBA–BSA was used as the hapten and the antibody (polyclonal; Ab 294) was produced by conjugating 3-((2-oxoethoxy)ethoxy) phenoxybenzoic acid and thyroglobulin (Ahn et al., 2007). For labeling the antibody with fluorescein isothiocyanate (FITC), 1 mg of the antibody in 1 ml of 0.05 M borate buffer (pH 8.5) was gently mixed with 12 μl of 1 mg ml^{-1} N-hydroxysulfosuccinimide fluorescein isothiocyanate (NHS-FITC) for 1 h at room temperature. Free fluorescein was removed by using a desalting column (PD-10, GE Health Care, Uppsala, Sweden). Phosphate buffered saline (PBS) buffer (1 × PBS; 8 g l^{-1} NaCl, 0.2 g l^{-1} KH_2PO_4, 1.2 g l^{-1} Na_2HPO_4, and 0.2 g l^{-1} KCl, pH 7.5) was used for the immunoassay.

2.3. Nanoparticles

Two hundred nanometer-fluorescent-carboxylated-polystyrene (PS)-nanoparticles (FC02F/8251, excitation: 360 nm, emission: 420 nm, Bangs Laboratories, Fishers, IN, USA) or 53 nm-fluorescent-carboxylated-PS-nanoparticles (FC02F/8684, excitation: 480 nm, emission: 520 nm, Bangs Laboratories) were used for testing the EPES or performing competitive immunoassays. The size of particles was measured by a dynamic light scattering (90Plus, Brookhaven Instruments, Holtsville, NY). The zeta potential of particles was measured by light scattering using a zeta potential analyzer (ZetaPlus, Brookhaven Instruments).

2.4. Competitive immunoassay for 3-PBA

A schematic of the 3-PBA competitive immunoassay is illustrated in Fig. S1. Two hundred nanometer-fluorescent-carboxylated-polystyrene (PS)-nanoparticles were washed two times with DI water to remove surfactant on the surface of particles. For passive adsorption of the 3-PBA–BSA to the nanoparticles, 160 μl of 2.6 mg ml^{-1} 3-PBA–BSA dissolved in PBS was mixed with 1 ml of 0.05% (w/v) fluorescent-carboxylated-PS-nanoparticles suspended in DI water and 840 μl of PBS. The mixing time proceeded for 2 h at room temperature, followed by overnight incubation at 4 °C. The mixed solution was then washed three times and finally suspended in DI water. To determine the minimum concentration of 3-PBA fluorescein labeled antibody needed for the competitive assay, the fluorescein labeled antibody was serially diluted with PBS by 10^{-3}–10^{-4} and tested on the 3-PBA–BSA coated fluorescent-carboxylated-PS-nanoparticles trapped into nanowells without free 3-PBA to compete. The results were then compared to the negative control using mouse-IgG conjugated with TRITC diluted by 10^{-3}. The 3-PBA analyte solutions mixed with the 3-PBA fluorescein labeled antibody at a 1:1 volume ratio (total 25 μl) was dropped onto the nanoarray where 200 nm-fluorescent-carboxylated-PS-nanoparticles–3-PBA–BSA were already accommodated. The nanoarray was then incubated for 30 min at room temperature followed by removal of the solution with the same method that was used to remove untrapped nanoparticles. The solution is removed by the Couette-flow that is established by the relative motion between the moving top plate and

stationary bottom plate. Concentrations of 3-PBA analyte were varied from 0 $\mu g\,l^{-1}$ to 10 $\mu g\,l^{-1}$ while the concentration of fluorescein labeled antibody was fixed.

2.5. Data analysis

The chip with the nanoarrays was placed on the stage of an inverted fluorescent microscope (TE300, Nikon, Tokyo, Japan) equipped with a CCD camera (Retiga 1300, QImaging, Canada) and interfaced with a computer and software for image acquisition. The images of the fluorescence were captured with a 40× objective lens. The intensities of fluorescence from the nanoarray were quantified by using ImageJ software (http://rsb.info.nih.gov/ij).

3. Results and discussion

3.1. Simulation of electrophoresis of a nanoparticle

A two-dimensional model of the electric field was developed with the electrostatics application mode from the AC/DC module in COMSOL Multiphysics (v. 3.5a; COMSOL Inc, Burlington, MA, USA). Fig. S2 shows the 2-D diagram of the EPES with boundary conditions used in the model. The model was used as a guide to designing the EPES system by estimating the efficiency of trapping of nanoparticles into wells.

The governing equation of the model is Gauss's law:

$$\nabla \cdot E = \frac{\rho}{\varepsilon_0} \tag{1}$$

where E is the electric field, ρ is the electric charge density, and ε_0 is the permittivity in a vacuum. A solution containing nanoparticles was approximated as pure water with permittivity of 80. Because the difference of permittivity between the polymethyl methacrylate (PMMA; 3.8) and lift-off layer (LOL; 3.0) was not significant, the coating layer of the photoresists was assumed to be a single layer of the PMMA. The electric field effects observed in the model were created by the difference in permittivity between the PMMA and solution. The boundary condition separating the PMMA and solution was represented as

$$n \cdot (\varepsilon_{r1} E_1 - \varepsilon_{r2} E_2) = 0 \tag{2}$$

$$n \times (E_1 - E_2) = 0 \tag{3}$$

where is $n$is a unit normal, ε_{r1} is the permittivity of water, ε_{r2} is the permittivity of PMMA, E_1 is the electric field in the water, and E_2 is the electric field in the PMMA. The components of electric field that were normal to the boundary were discontinuous while the others were continuous. The indium tin oxide layer (ITO) was modeled as a perfectly conductive material at the top and bottom side. The top conductor was set to ground (i.e. $V=0$ V) and the bottom conductor was defined with several different voltages. The left and right edges of the model were set to the reflecting/symmetry condition.

$$n \cdot E = 0 \tag{4}$$

Given that the x component of electric field was constant relative to the y component, and only becomes large in close proximity to the PMMA, the velocity of the particle could be calculated using a one dimensional model. The displacement of a particle was calculated by solving the differential equation (Eq. (5)) with MATLAB (v. 2009b, Natick, MA).

$$m\ddot{x} = F_E + F_G - F_{Drag} \tag{5}$$

where m is the particle mass, $\ddot{x}$ is the particle acceleration, F_E is the force due to the electric field, F_G is the force due to gravity, and F_{Drag} is the drag force. The scale of the EPES ensured a low Reynolds number and laminar flow, therefore the drag equation was approximated with Stokes drag, leading to

$$m\ddot{x} = qE + mg - 6\pi r\mu\dot{x} \tag{6}$$

where μ is the dynamic fluid viscosity, r is the particle radius, q is the charge on a particle, and E is the average electric field in the device. Eq. (6) was solved for the velocity change of three different charged particles with diameters of 56 nm, 93 nm, and 220 nm as a function of time and voltage drop. All particles showed a linear relationship between voltage drop across the device and maximum velocity of the particle (Fig. S3)

The electric field lines in the EPES were simulated with the finite element package COMSOL (Fig. 1). The size of the well was 230 nm and the spacing between two wells was 4 μm. The electric field lines indicate that the negatively charged particles will move into the well where the electric potential was maximum.

3.2. Entrapment of nanoparticles in channels and wells

Scanning electron microscope (SEM) images of nano-patterned arrays and the schematic of the EPES system are shown in Fig. 2a–c. The EPES consisted of a patterned PMMA–LOL 2000-ITO–glass slide (bottom) and a plain ITO–glass slide (top). The ITO at the bottom of a well or channel was used as the electrode. The slides were each equipped with micro-scale manipulators to precisely control the location of the top and bottom slides horizontally or vertically. To create perpendicular electrophoretic forces, the bottom slide was connected to the positive terminal while the top slide was connected to the ground terminal. The nanoparticle–water solution was added to the surface of the patterned bottom slide as a droplet. The upper ITO–glass slide was then placed onto the droplet. The distance between two slides was 490 μm.

The limited resolution of the optical microscope prevented the imaging of nanowells with less than 100 nm-size. Larger structures were required so that optical imaging of the particles was possible—therefore channels that offer a much larger trapping area rather than corresponding nanowells of a similar dimension were used for initial assessment of the EPES techniques. Nanowells were used for the actual immunoassays.

In order to demonstrate size-dependent-particle trapping using the EPES, 53 nm-fluorescent-carboxylated-polystyrene particles (with a green fluorescence emission) and 200 nm-fluorescent-carboxylated-polystyrene particles (blue emission) were dropped onto nanochannels: one set of channels had width of 150 nm, the other channel had a width of 230 nm with 2 μm spacing between the two channels (Fig. 3a). The larger particles were added to the nanochannels and were trapped into the larger channels; this application was followed by the smaller particles that were then directed by the electrical field into the smaller channels. The larger channels were fully occupied and could not accommodate any smaller particles. The surface charge of the suspended particles was negative due to the carboxyl terminal group on the particles. The zeta potential of the 53 nm- and 200 nm-nanoparticles was -39.0 ± 1.4 mV and -55.0 ± 1.2 mV respectively. After placing the top ITO–glass slide onto the droplet of particle solution and turning on the voltage, negatively charged particles migrated toward the surface of opposite electrical polarity.

The EPES was operated for 1 h for a given concentration of particle solution; the long time ensured complete occupation of all the wells by particles. The applied voltage was 2.133 V which was measured on the surface of the patterned slide by using a multimeter. All particles were trapped respectively into the channels based on their size and there were few particles that were non-specifically bound to the surface of the PMMA (Fig. 3a). After trapping, the remaining solution on the array was removed by the Couette flow that was established by moving the top

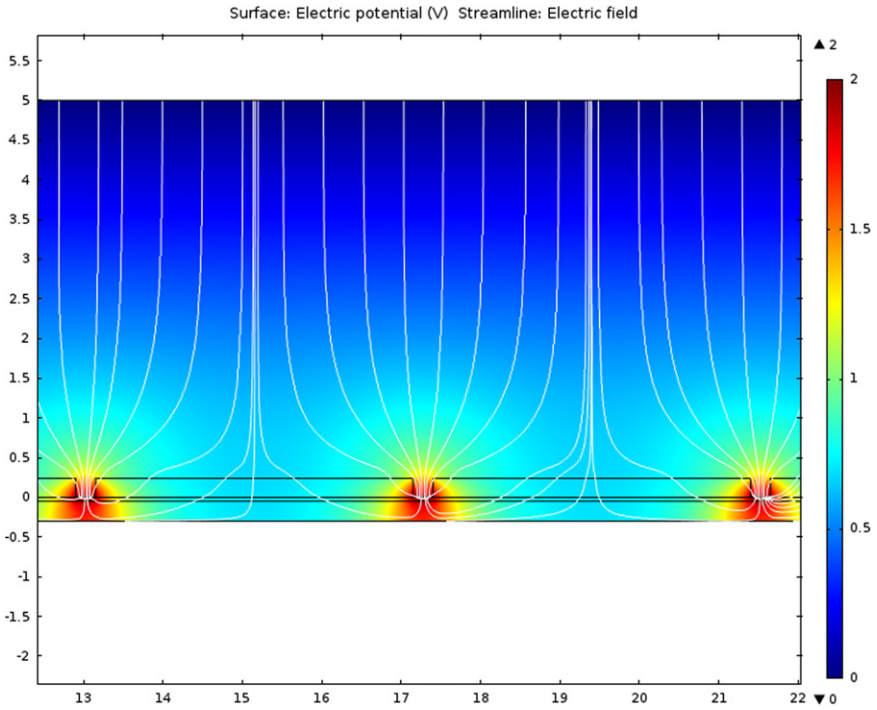

Fig. 1. Simulated electric field lines (white solid lines) for the EPES. For the applied potential of 2 V (DC), electric field lines showed that the negatively charged particles will find the ITO surface at the bottom of the wells, as the potential there was maximum.

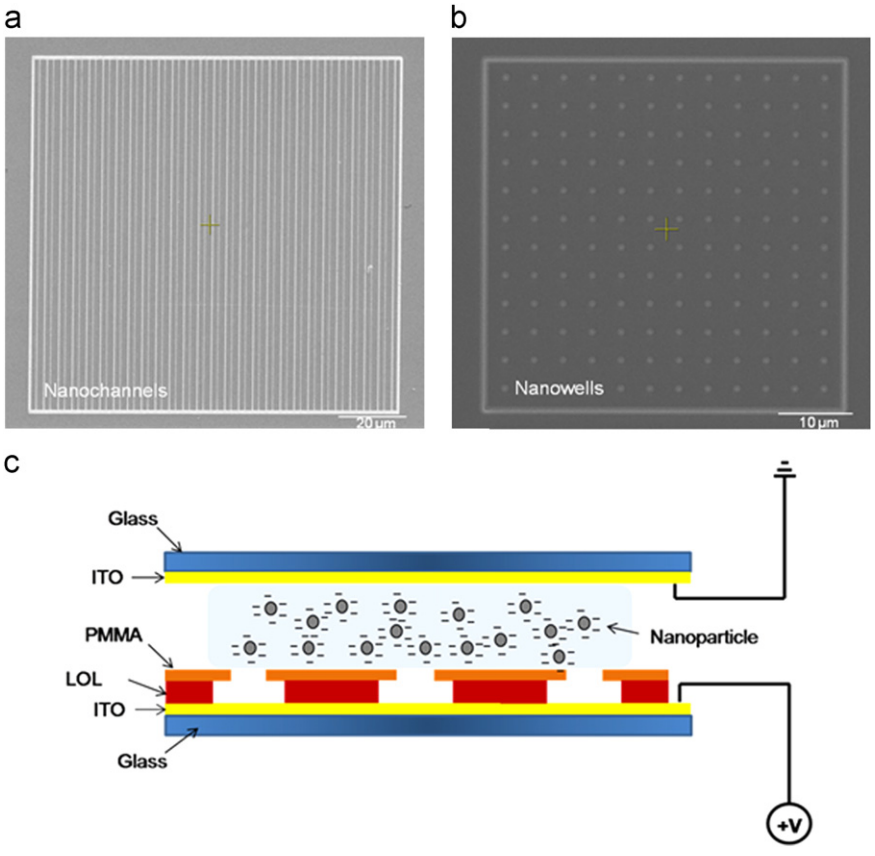

Fig. 2. Nanoarrays and the EPES. (a) Scanning electron microscope (SEM) images of the nanochannels; total of 52 nanochannels on a 100 μm × 100 μm square. The widths of the channels are 150 nm and 230 nm respectively. The spacing between the channels is 2 μm, (b) nanowells; 12 × 12 array on a 50 μm × 50 μm square. The diameter of the wells is 230 nm and the spacing between the wells was 4 μm, (c) The schematic of the EPES; the ITO surface of the patterned PMMA–LOL–ITO–glass slide (bottom) is connected to the positive terminal while the ITO surface of the ITO–glass slide (top) is connected to the ground terminal. The thickness of LOL 2000 and PMMA is 155 nm and 85 nm respectively. The solution between the slides consists of the negatively charged nanoparticles and deionized (DI) water.

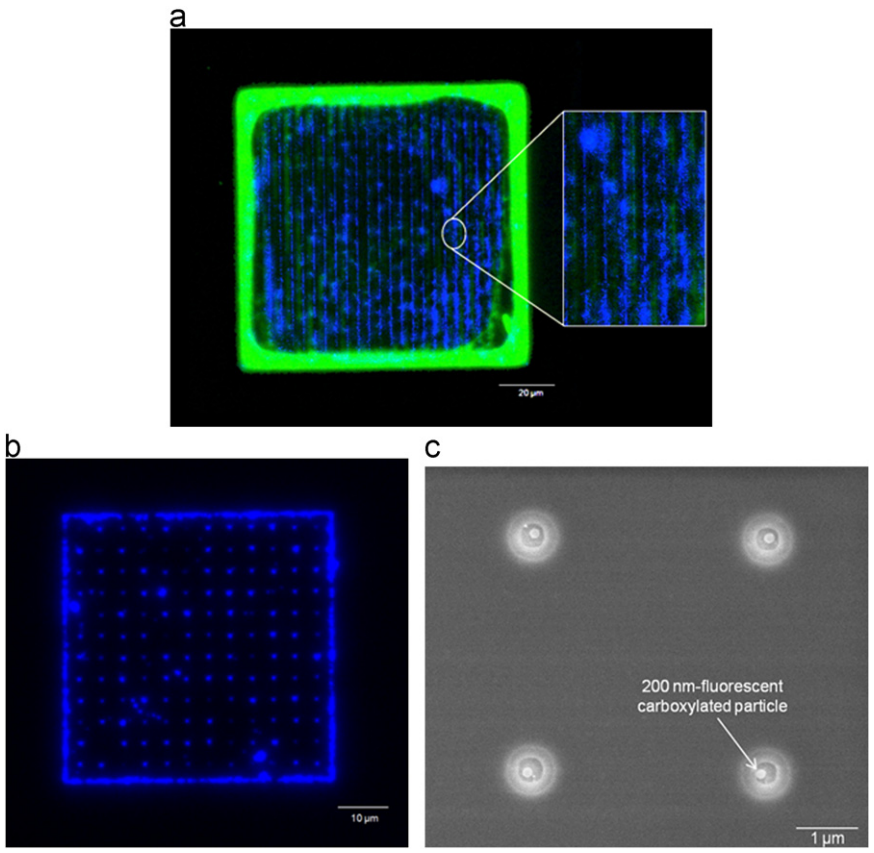

Fig. 3. Entrapment of the nanoparticles in the nanoarrays using the EPES. (a) Nanochannels; 200 nm-fluorescent-carboxylated-PS particles (blue emission) and 53 nm-fluorescent-carboxylated-PS particle (green emission) are trapped respectively into 230 nm- or 150 nm-width-channels; Some channels shown as green and blue lines are magnified with small rectangle, (b) fluorescent image of nanowells and (c) SEM image of nanowells −200 nm fluorescent-carboxylated-PS particles are trapped into 230 nm-wells. (For interpretation of the references to color in this figure legend, the reader is referred to the web version of this article.)

ITO–glass slide relative to the bottom slide while the voltage was still on. There was no additional rinsing procedure for removing non-specifically bound particles.

Following successful optimization of conditions with the nanochannels, a similar procedure was performed with the nanowells that were used for immunoassays. For the same trapping period and voltage, 200 nm-fluorescent-carboxylated-polystyrene particles were successfully trapped into the nanoarray that consisted of 230 nm-wells with 4 μm-horizontal and vertical spacing although the trapping area decreased significantly compared to the nanochannels (Fig. 3b and c). The trapping efficiency was 99%, estimated by counting the fraction of the wells where nanoparticles were trapped (91% of wells contained a single particle, 8% of wells contained two or more particle and 1% of wells were empty). In order to achieve a reproducible immunoassay, it is important to have reliable and controlled deposition of particles conjugated with biological molecules into nanowells. The reproducibility and variance can be improved if the nanoarrays have a defined number of nanoparticles. In order to achieve this goal, we optimized parameters to attain single particle occupancy of the nanowells. For 200 nm-particles, a width of 230 nm and depth of 240 nm of the well resulted in 91% single particle-occupancy as noted above and as illustrated in Fig. 3c. Non-specific binding of the particles on the PMMA was not significant.

3.3. *Detection of 3-PBA on the nanoarray with the electrophoretic particle entrapment system*

Fig. 4a–e shows the immunofluorescent images of the nanostructured arrays following competitive immunoassays with five different concentrations of 3-PBA target analyte dissolved in PBS: 0, 0.01, 0.1, 1, and 10 $\mu g\,l^{-1}$. The concentration of the 3-PBA fluorescein-labeled antibody used for the competitive assay was $0.286 \times 10^{-4}\ \mu g\ \mu l^{-1}$. At this concentration, there was a statistically significant difference between each of the concentrations compared to the negative control using anti-mouse IgG conjugated with TRITC ($p < 0.05$) (Fig. S4a–c). The fluorescent intensity was collected from the detection area of the array (50 μm × 50 μm; white broken line in Fig. 4a). The relative fluorescent intensity of the 3-PBA fluorescein labeled antibody was used to create a standard curve by normalization with the fluorescent intensity of the nanoparticles trapped into the wells. Data points were acquired respectively from at least four random replicates out of the nine arrays with the same experimental conditions. Immunocomplexes emitted consistent fluorescein signals (bottom images in Fig. 4) compared to the particle themselves. This can be attributed to the uniform coating of the hapten on the surface of the particle and strong binding of 3-PBA fluorescein-labeled antibody to the particle–hapten in the wells during the immunoassay. On the other hand, the interchelation of the fluorescent dyes into the commercialized particles during manufacturing is apparently variable, leading to the inconsistent fluorescent signal observed in the top images in Fig. 4.

The normalized fluorescent intensity decreased with increasing concentration of 3-PBA and then leveled off at 1 $\mu g\,l^{-1}$, showing that binding of the 3-PBA antibody to the 3-PBA–BSA coated on the surface of the nanoparticles was inhibited by free 3-PBA (Table 1) through competition. In the standard curve (Fig. 5), the limit of detection was 0.0064 $\mu g\,l^{-1}$ which was 30 pM based on the molecular weight of 3-PBA at 214.2 g mol^{-1} (Morgan et al., 2007). The linear detection range was 0.0064 $\mu g\,l^{-1}$–1 $\mu g\,l^{-1}$ with an R^2 of

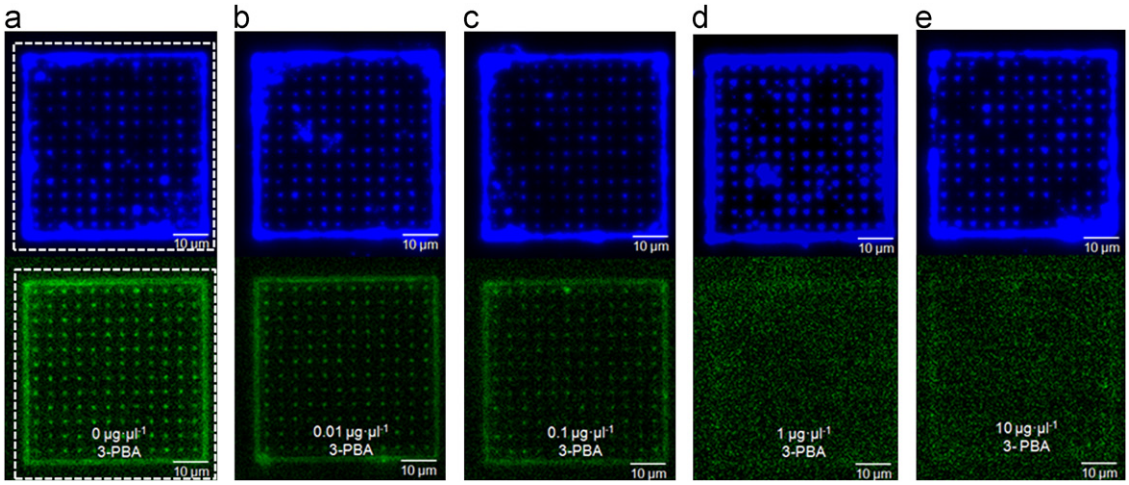

Fig. 4. Immunofluorescent images of the nanoarrays in the 3-PBA competitive immunoassay. The concentration of the 3-PBA: (a) 0 μg l^{-1}, (b) 0.01 μg l^{-1}, (c) 0.1 μg l^{-1}, (d) 1 μg l^{-1}, and (e) 10 μg l^{-1}. Top images (blue emission): the nanoarray with only 200 nm-fluorescent-carboxylated-PS particles coated with 3-PBA–BSA; bottom images (green emission): the nanoarray after adding mixed solutions of 3-PBA and the fluorescein labeled antibody for the competitive immunoassay. White broken line indicates detection area (50 μm × 50 μm) where the emited fluorescent signal was obtained. (For interpretation of the references to color in this figure legend, the reader is referred to the web version of this article.)

Table 1
The data points used in the standard curve.

Concentration of 3-PBA target (μg/l)	I/I_0	SD
0	0.277	0.009
0.01	0.233	0.040
0.1	0.154	0.049
1	0.072	0.016
10	0.073	0.021

I: Fluorescent intensity of the fluorescein labeled antibody bound to the 3-PBA–BSA coated on the fluorescent-carboxylated-PS particles trapped to the nanowells, I_0: fluorescent intensity of the fluorescent-carboxylated-PS particles trapped to the nanowells, SD: standard deviation from at least four replicates.

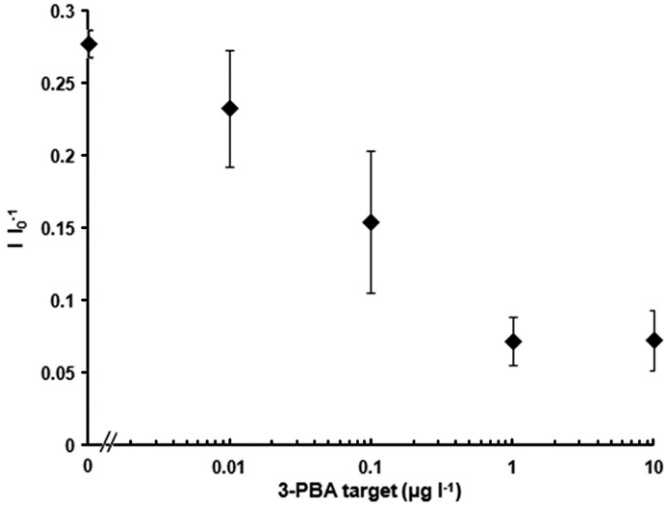

Fig. 5. Immunofluorescent intensities of the fluorescein labeled antibody bound to the 3-PBA–BSA coated on fluorescent-carboxylated-PS particles trapped into the nanowells after the competition with 3-PBA (0–10 μg l^{-1}). I: fluorescent intensity of the fluorescein labeled antibody (excitation wavelength: 480 nm, emission wavelength: 520 nm), I_0: fluorescent intensity of the particles (excitation: 360 nm, emission: 420 nm) trapped into the nanowells. The standard curve represents the average of at least four replicates with their standard deviation. The slope of the linear detection range was 0.035 with R^2 0.9999.

0.9999. The half maximal inhibitory concentration (IC_{50}) was 0.15 μg l^{-1}.

The modeling results showed that it should be possible to collect a large fraction of the particles in solution in wells. An estimate of the electrophoretic mobility using the measured zeta potential indicated that it would take about 10 s for a nanoparticle to traverse the entire width of the microchannel that contained the particle suspension. However, the simple model ignores issues such as Brownian motion of the particles (the mean displacement could be 2 μm in 10 s). In addition, particles near the wells may act to repel additional particles from accumulating in the wells. Therefore, the actual maximum velocity of particles and optimal trapping time required further refinement using numerical modeling.

The modeling results showed that the vector direction of the electric field was independent of the field gradient, and was only affected by the geometry of the array. Therefore, charged particles coated with the biological reagents can be trapped with a low voltage. In our study, 2 V was sufficient to trap nanoparticles that were conjugated with 3-PBA–BSA. Furthermore, by optimally designing the spacing between wells, the fraction of particles that were trapped can be increased, resulting in less waste of particles conjugated with valuable biological reagents. The modeling results provided useful information about the trapping time, optimal voltage, and design of the array for effective use of the particles.

The nanoparticles were trapped into their corresponding nanochannels based on the size of particles, and this was demonstrated by channels showing different fluorescent emission. There was no co-location of the fluorescent signal, showing that the particles were specifically trapped in their corresponding channel. This size-dependent-particle-trapping using the EPES suggested that multiplexing of the system is possible by sequential addition of nanoparticles of select sizes that correspond the target channel, or well. Furthermore, based on the observations that 200 nm-fluorescent-carboxylated-PS particles were trapped in a nanowell where the parking area is much less than that of nanochannel, the efficiency of trapping particles into their assigned location using the EPES was highly affected by removing particles bound non-specifically to the surface of the PMMA, due to the low affinity of highly carboxylated particles (Han et al., 2007; Ware et al., 1991) for the hydrophilic PMMA. The weak binding interaction between the particles and

PMMA enabled simple rinsing by moving the solution slowly without using any additional chemicals or buffers.

A competitive assay for 3-PBA in the EPES showed enhanced sensitivity compared to a previously reported ELISA (Shan et al., 2004), with a sixteen-fold improvement in the limit of detection that was achieved without the use of sophisticated optical detection technology. Although the image analysis of the immunofluorescence used in our study was not a sophisticated approach, the nanostructured arrays nevertheless demonstrated an improved sensitivity in a short time (20 min incubation time), driven by (1) use of a minimal amount of 3-PBA–BSA or 3-PBA fluorescein-labeled antibody, leading to reduced diffusion time that has been a barrier in immunoassays with surface immobilization of capture antibodies (Lynch et al., 2004), (2) enhanced adsorption of analyte to the surface of the antibody-bearing nanoparticles in wells due to the impact of curvature on adsorption to a surface (Jiang et al., 2008), (3) increased fluorescent signal due to light diffraction from the grating that is created by the nanostructures on the surface (Goh et al., 2003) and (4) the high affinity of the antibody to 3-PBA hapten (Ahn et al., 2007).

4. Conclusion

The EPES/nanoarray system is a simple and sensitive sensor platform for the detection of biological analytes. EPES solves the problem of locating biological molecules at multiple sites on an array with nanometer scale precision, yet with a simple, relatively straightforward and economically attractive method. The size and location of the binding sites can be easily controlled, in principle enabling a range of different particle sizes to be trapped at different locations on the chip with the ensuing ability to perform multiplexed assays. In addition, by using the fluorescent intensity of the nanoparticles trapped into the wells as an internal standard, corrected relative values for the quantification of the analyte can be obtained under various experimental conditions that may include, for example, variable sensitivities of the detection system.

Acknowledgments

The authors thank the Northern California Nanotechnology Center at the University of California, Davis for the facilities used in the fabrication of nanoarrays and Professor. T. Young for permission to use his dynamic light scattering and Zeta potential analyzer. We thank Professor A. Barakat for permission to use his inverted fluorescent microscope. Professor B. Hammock is a George and Judy Marcus Senior Fellow of the American Asthma Foundation. This project described was supported by Award no. P42ES004699 from the National Institute of Environmental Health Sciences. The content is solely the responsibility of the authors and does not necessarily represent the official views of the National Institute of Environmental Health Sciences or the National Institutes of Health. The support of the Western Center for Agricultural Health and Safety at the University of California Davis, No. PHS OH07550 is also acknowledged. This work was also supported by Grant no. 200911634 from the NIAID, NIH. Additional support was provided by the National Research Initiative of the USDA Cooperative State Research, Education and Extension Service, Grant no. 2009-35603-05070.

Appendix A. Supplementary materials

Supplementary data associated with this article can be found in the online version at http://dx.doi.org/10.1016/j.bios.2012.08.042.

References

Ahn, K.C., Lohstroh, P., Gee, S.J., Gee, N.A., Lasley, B., Hammock, B.D., 2007. Analytical Chemistry 79, 8883–8890.
Chan, S.M., Ermann, J., Su, L., Fathman, C.G., Utz, P.J., 2004. Nature Medicine 10, 1390–1396.
Chang, C.-Y., Takahashi, Y., Murata, T., Shiku, H., Chang, H.-C., Matsue, T., 2009. Lab on a Chip 9, 1185–1192.
Ginger, D.S., Zhang, H., Mirkin, C.A., 2004. Angewandte Chemie 43, 30–45.
Goh, J.B., Tam, P.L., Loo, R.W., Goh, M.C., 2003. Analytical Biochemistry 313 (2), 262–266.
Han, J.-H., Kim, K.-Y., Yoon, J.-Y., 2007. Analytica Chimica Acta 584, 252–259.
Haukanes, B.I., Kvam, C., 1993. Bio-Technology 11 (1), 60–63.
Jiang, W., Kim, B.Y.S., Rutka, J.T., Chan, W.C.W., 2008. Nature Nanotechnology 3, 145–150.
Juan, M., Gordon, R., Pang, Y., Eftekhari, F., Quidant, R., 2009. Nature Physics 5, 915–919.
Kusnezow, W., Syagailo, Y.V., Ruffer, S., Baudenstiel, N., Gauer, C., Hoheisel, J.D., Wild, D., Goychuk, I., 2006. Molecular and Cellular Proteomics 5 (9), 1681–1696.
Laffin, B., Chavez, M., Pine, M., 2010. Toxicology 267, 39–44.
Lee, K.B., Kim, E.-Y., Mirkin, C.A., Wolinsky, S.M., 2004. Nano Letters 4, 1869–1872.
Liu, Y., Ke, Y., Yan, H., 2005. Journal of the American Chemical Society 127, 17140–17141.
Lynch, M., Mosher, C., Huff, J., Nettikadan, S., Johnson, J., Henderson, E., 2004. Proteomics 4, 1695–1702.
Morgan, M.K., Sheldon, L.S., Croghan, C.W., Jones, P.A., Chuang, J.C., Wilson, N.K., 2007. Environmental Research 104, 226–274.
Powell, T., Yoon, J.-Y., 2006. Biotechnology Progress 22, 106–110.
Salaita, K., Lee, S.W., Wang, X., Huang, L., Dellinger, T.M., Liu, C., Mirkin, C.A., 2005. Small 10, 940–945.
Sanedrin, R.G., Amro, N.A., Rendlen, J., Nelson, M., 2010. Nanotechnology 21, 1–7.
Schwartz, D.K., 2001. Annual Review of Physical Chemistry 52, 107–137.
Shan, G., Huang, H., Stoutamire, D.W., Gee, S.J., Leng, G., Hammock, B.D., 2004. Chemical Research in Toxicology 17, 218–225.
Sharma, S.K., Tyagi, P.K., Upadhyay, A.K., Haque, M.A., Mohanty, S.S., Raghavendra, K., Dash, A.P., 2009. Acta Tropica 112, 181–187.
Ueyama, J., Kimata, A., Kamijima, M., Hamajima, N., Ito, Y., Suzuki, K., Inoue, T., Yamamoto, K., Takakgi, K., Saito, I., Miyamoto, K.-I., Hasegawa, T., Kondo, T., 2009. Environmental Research 109 (2), 175–180.
Ware, J.A., Kang, J., DeCenzo, M.T., Smith, M., Watkins, S.C., Slayter, H.S., Saitoh, M., 1991. Blood 78 (7), 1713–1721.
Wilson, R., Cossins, A.R., Spiller, D.G., 2006. Angewandte Chemie International Edition 45 (37), 6104–6117.
Zaim, M., Aitio, A., Nakashima, N., 2000. Medical and Veterinary Entomology 14, 1–5.